Apaf1 plays a pro-survival role by regulating centrosome morphology and function

Elisabetta Ferraro[1,2,*], Maria Grazia Pesaresi[3], Daniela De Zio[2], Maria Teresa Cencioni[4], Anne Gortat[5], Mauro Cozzolino[3], Libera Berghella[6], Anna Maria Salvatore[7], Bjorn Oettinghaus[8], Luca Scorrano[8], Enrique Pérez-Payà[5] and Francesco Cecconi[1,2,‡]

[1]Laboratory of Molecular Neuroembryology, IRCCS Fondazione Santa Lucia, 00143, Rome, Italy
[2]Dulbecco Telethon Institute, Department of Biology, University of Rome 'Tor Vergata', 00133, Rome, Italy
[3]Laboratory of Neurochemistry, IRCCS Fondazione Santa Lucia, 00143, Rome, Italy
[4]Laboratory of Neuroimmunology, IRCCS Fondazione Santa Lucia, 00143, Rome, Italy
[5]Department of Medicinal Chemistry, Centro de Investigación Príncipe Felipe, 46012 Valencia, Spain and IBV-CSIC, E-46010, Valencia, Spain
[6]Hospital San Raffaele Sulmona, 67039, Sulmona (AQ), Italy
[7]Institute of Neurobiology and Molecular Medicine, CNR 00137, Rome, Italy
[8]Department of Cell Physiology and Metabolism, University of Geneva, 1206, Geneva, Switzerland

*Present address: Laboratory of skeletal muscle development and metabolism, IRCCS San Raffaele, 00163 Rome, Italy
‡Author for correspondence (francesco.cecconi@uniroma2.it)

Accepted 27 June 2011
Journal of Cell Science 124, 3450–3463

doi: 10.1242/jcs.086298

Summary

The apoptotic protease activating factor 1 (Apaf1) is the main component of the apoptosome, and a crucial factor in the mitochondria-dependent death pathway. Here we show that Apaf1 plays a role in regulating centrosome maturation. By analyzing Apaf1-depleted cells, we have found that Apaf1 loss induces centrosome defects that impair centrosomal microtubule nucleation and cytoskeleton organization. This, in turn, affects several cellular processes such as mitotic spindle formation, cell migration and mitochondrial network regulation. As a consequence, Apaf1-depleted cells are more fragile and have a lower threshold to stress than wild-type cells. In fact, we found that they exhibit low Bcl-2 and Bcl-X_L expression and, under apoptotic treatment, rapidly release cytochrome *c*. We also show that Apaf1 acts by regulating the recruitment of HCA66, with which it interacts, to the centrosome. This function of Apaf1 is carried out during the cell life and is not related to its apoptotic role. Therefore, Apaf1 might also be considered a pro-survival molecule, whose absence impairs cell performance and causes a higher responsiveness to stressful conditions.

Key words: Apaf1, Centrosome, Microtubules

Introduction

The apoptotic protease activating factor 1 (Apaf1) is one of the most studied proapoptotic proteins. It is the core of the apoptosome, which is formed upon triggering of the mitochondrial apoptotic pathway. Following an apoptotic induction, cytochrome *c* is released from mitochondria, it binds Apaf1 and induces a conformational change of this protein, which is able to oligomerize and to recruit and activate procaspase-9 (Zou et al., 1997). Recently, Kroemer and coworkers have identified a novel role for Apaf1, which is independent of its function in the cell death machinery. Indeed, they have found that Apaf1 is involved in the maintenance of genomic stability upon DNA damage (Mouhamad et al., 2007; Zermati et al., 2007).

The centrosome is a major microtubule-organizing center (MTOC) in animal cells. Microtubules mainly nucleate from the surface of centrosomes, which are formed by a pair of centrioles surrounded by a pericentriolar material. One of several proteins forming the pericentriolar material is γ-tubulin; it catalyzes the nucleation of microtubule polymers from α–β-tubulin dimers. In association with several gamma complex proteins (GCPs), γ-tubulin can form two complexes, namely a small γ-TuSC (γ-tubulin small complex) and a large ring-shaped complex, γ-TuRC (γ-tubulin ring complex). γ-Tubulin moves from the cytosol to the centrosomes, the recruitment of γ-tubulin to the centrosomes being regulated by kinases, by proteins of the pericentriolar material and by a protein binding the γ-TuRC called NEDD1 (neural precursor cell expressed, developmentally downregulated 1) (Haren et al., 2006; Luders et al., 2006; Oegema et al., 1999). Recently it has been found that the hepatocellular carcinoma antigen 66 (HCA66), which had been previously described as an interactor of Apaf1 and a positive regulator of Apaf1-dependent apoptosis (Piddubnyak et al., 2007), is required for the stability of γ-TuSC proteins and that its deficiency affects spindle microtubule assembly (Fant et al., 2009).

Centrosomes are important for division: during S phase, the centrosome duplicates and the two centrosomes separate to form the poles of the mitotic spindle. At this point, γ-tubulin recruitment to each centrosome increases; this enhances the centrosome microtubule nucleation capacity and a microtubule aster is formed. Following nuclear envelope breakdown, microtubules originated from centrosomes, attach to the kinetochores of chromosomes, and mitosis can proceed (Fukasawa, 2007; Jaspersen and Stearns, 2008; Mazia, 1987).

Microtubules and centrosomes also play an important role in cell migration, which is a process stringently regulated during

tissue development, chemotaxis and wound healing (Kodani and Sutterlin, 2008; Noritake et al., 2005; Watanabe et al., 2005). Moreover, the microtubule cytoskeleton is essential for the organization and movement of organelles such as the Golgi complex (Thyberg and Moskalewski, 1999). The distribution and organization of the endoplasmic reticulum (ER) also depends on interactions with microtubules, and one level of regulation of mitochondria (besides fission and fusion) is their active transport along microtubules (Jahani-Asl et al., 2010; Park and Blackstone, 2010). In addition, microtubules are essential for vesicle transport, because vesicles use the microtubule network to meet and fuse with several different endocytic organelles (Hehnly and Stamnes, 2007). Besides their function as organizers of the cytoskeleton and the mitotic spindle, centrosomes serve also as spatiotemporal organizers of events regulating cell cycle, probably by triggering G1 to S transition checkpoints (Rai et al., 2008; Rieder et al., 2001).

In this paper, we show that Apaf1 has a role in centrosome stability, because it favors the recruitment of HCA66, the stabilizer of the γ-TuSC, to the centrosomes. In the absence of Apaf1, association of HCA66 with the centrosomes is poor; aberrant centrosomes are thus formed and this impairs microtubule nucleation. We also show that, as a consequence of Apaf1 deficiency, several biological processes are affected, such as the formation of a normal bipolar mitotic spindle, cell division, cell migration and mitochondrial network organization. Moreover, anti-apoptotic proteins are downregulated in Apaf1-depleted cells, which, in fact, rapidly release cytochrome *c* upon apoptotic treatment. For these reasons, we suggest that the absence of Apaf1 makes cells more fragile and more sensitive to stress. Thus, from this viewpoint, Apaf1 has to be also considered a pro-survival protein in addition to its pro-apoptotic role.

Results

Apaf1-deficient cells release cytochrome *c* with a faster kinetics than that of WT cells

We have previously reported that Apaf1-deficient proneural ETNA [embryonic telencephalic naïve *Apaf1* knockout (*Apaf1*-KO)] and ETNA cells overexpressing a dominant-negative form of caspase-9 (C9DN-ETNA) – two cell lines devoid of a functional apoptosome and therefore resistant to apoptosis – are both able to survive with an active metabolism for a long time before undergoing a non-apoptotic form of cell death (Ferraro et al., 2008). By continuous analysis of the behavior of these two apoptosome-deficient cell lines, we made a challenging observation: upon apoptotic treatment with tunicamycin (an inhibitor of *N*-linked glycosylation) plus the proteasome inhibitor MG132, which is needed to avoid cytochrome *c* degradation after its release, many more ETNA KO cells than C9DN-ETNA cells released cytochrome *c* (Fig. 1A,E).

In order to understand whether this difference was due to the overexpression of the dominant-negative form of caspase-9 or to the absence of Apaf1, we performed the same kind of analysis on wild-type ETNA cells (ETNA WT). We observed that WT cells behaved like C9DN-ETNA cells and showed, upon apoptotic treatment, a much lower release of cytochrome *c* than *Apaf1*-knockout cells (Fig. 1A,E). Accordingly, as reported in Fig. 1B, the percentage of cells with dissipated mitochondrial membrane potential ($\Delta\Psi$m) (Fig. 1B Tun; red line, left peak) was notably higher in *Apaf1*$^{-/-}$ cells compared with ETNA-WT and C9DN-ETNA cells under the same apoptotic treatment. Such a difference between Apaf1-deficient ETNA cells and WT and C9DN-ETNA cells indicated that the faster kinetics of cytochrome *c* release was not due to the absence of a functional apoptosome or to the overexpression of C9DN but, instead, to the absence of Apaf1.

To ascertain whether the high susceptibility to mitochondrial damage was a general consequence of Apaf1 depletion or whether it was merely a clonal effect, we analyzed other SV40 antigen-transformed cell lines, i.e. Apaf1-depleted and wild-type immortalized mouse embryonic fibroblasts (I-Mefs KO and I-Mefs WT). Also in this context we found, in mutant cells under tunicamycin treatment, many more cytochrome-*c*-releasing cells and cells with depolarized mitochondria when compared with WT cells (Fig. 1C–E). As an alternative pro-apoptotic stimulus, we used the mRNA transcription inhibitor actinomycin D and confirmed the difference between *Apaf1*-KO and WT genotypes, which, we conclude, was not dependent on the apoptotic stimulus used (Fig. 2). Interestingly, also under normal conditions (where very rare spontaneous apoptotic cells are generally found) more cytochrome-*c*-releasing cells are detectable in *Apaf1*-KO I-Mefs (Fig. 2, I-Mefs KO Ctrl, arrow).

Therefore, these experiments suggest that Apaf1-deficient cells are more sensitive than WT cells to apoptotic insults.

Anti-apoptotic proteins are downregulated in Apaf1-deficient cells

In order to understand why the absence of Apaf1 makes cells more susceptible to mitochondrial damage we analyzed expression levels of the anti-apoptotic proteins Bcl-2 and Bcl-X_L. Both proteins belong to the Bcl-2 family, which is in charge of regulating mitochondrial outer membrane permeabilization (MOMP) and, as a consequence, cytochrome *c* release from mitochondria (Danial and Korsmeyer, 2004). Interestingly, in line with our observations, we found that the expression of these anti-apoptotic proteins is lower in all Apaf1-deficient cell lines analyzed than in their WT counterparts (Fig. 3A,B). In ETNA cells the absence of Bcl-2 downregulation might be compensated by the strong downregualtion of Bcl-X_L expression in the balance between genes that control apoptosis (Lotem and Sachs, 1995).

Because Bcl-2 and Bcl-X_L might be transcriptionally regulated (Catz and Johnson, 2001; Sevilla et al., 2001) we also checked, by means of a quantitative real-time PCR analysis of their mRNA levels, whether their downregulation was also evident at a transcriptional level. We found that the lower expression of Bcl-2 and Bcl-X_L was also due to a transcriptional downregulation (Fig. 3B). To confirm the effect of Apaf1 deficiency on Bcl-2 and Bcl-X_L expression, we went on to evaluate the amount of both proteins in mouse embryonic brains [embryonic day (E)14.5] and we found that both protein and mRNA levels were downregulated in Apaf1-deficient embryos as well (Fig. 3A–C).

Therefore, *Apaf1*-KO cells express low amount of anti-apoptotic proteins, which might explain their lower threshold in MOMP regulation.

Along with a fast kinetics of cytochrome *c* release, Apaf1-deficient cells show mitochondrial fragmentation

Because Apaf1-depleted cells show fast kinetics of cytochrome *c* release, and because release of cytochrome *c* has been proposed to be favored by mitochondrial fission [although the debate on this topic is still open (reviewed by Scorrano, 2009)], we set out

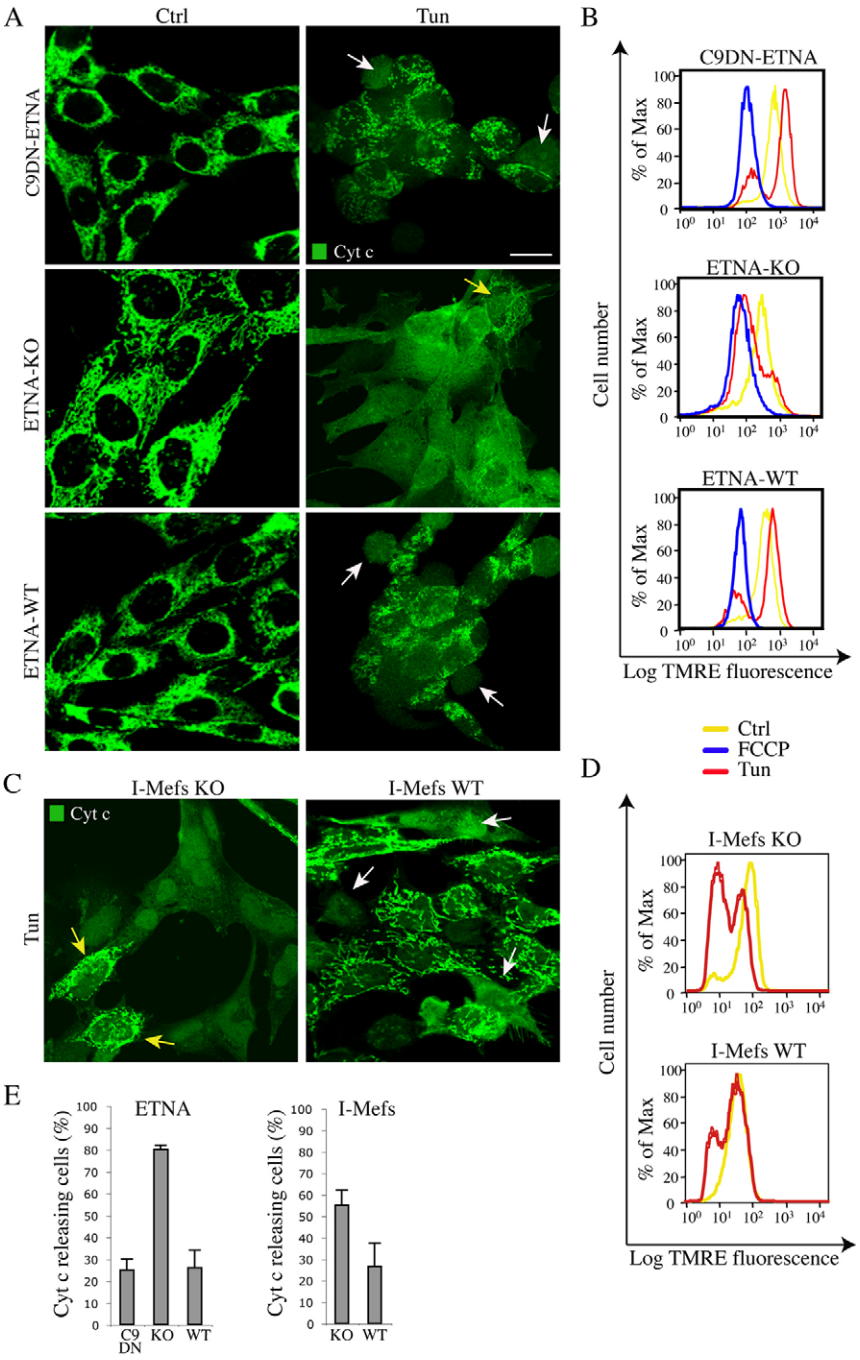

Fig. 1. Fast kinetics of cytochrome *c* release and $\Delta\Psi$m dissipation in Apaf1-depleted cells.
(**A**,**C**) Immunofluorescence staining for the detection of cytochrome *c* (green) in C9DN-ETNA, ETNA KO and ETNA WT cells untreated (Ctrl) or treated with 3 μg/ml tunicamycin plus 2 μM MG132 for 40 hours (Tun; A) and in I-Mefs KO and I-Mefs WT cells treated for 20 hours with 2 μg/ml tunicamycin (Tun; C). White arrows indicate cells with cytochrome *c* released into the cytosol, and yellow arrows indicate cells with cytochrome *c* within the mitochondria. Notably, when ETNA-WT, C9DN-ETNA and ETNA KO cells were treated with the caspase inhibitor Q-VD-OPH, to avoid cell detachment from the dish, the same results were obtained (data not shown). Scale bar, 20 μm. (**B**) C9DN-ETNA, ETNA KO and ETNA WT and (**D**) I-Mefs KO and I-Mefs WT cells untreated (Ctrl, yellow curve), treated with 10 μM carbonyl cyanide-*p*-trifluoromethoxyphenylhydrazone (FCCP; an uncoupler that dissipates the transmembrane potential by preventing the generation of a proton gradient, used as a control for mitochondrial depolarization; blue curve) or treated with tunicamycin (Tun, red curve) were stained with 50 nM tetramethylrhodamine ethyl ester (TMRE, MolecularProbes) for 10 minutes, washed and then analyzed by flow cytometry on a FACScan (Becton Dickinson) in FL-2 for $\Delta\Psi$m measurement. Note that in ETNA KO cells there is a marked depolarization of the mitochondria (Tun, red curve). (**E**) Quantitative analysis of the number of cells releasing cytochrome *c* upon the treatments described in A and C, and represented by histograms each indicating the means ± s.e.m. of three independent experiments. In all, at least 100 cells were analyzed in each field examined and five randomly chosen fields for each experimental condition were counted.

to establish whether the mitochondrial network in *Apaf1*-KO cells was altered. By staining mitochondria in untreated WT and *Apaf1*-KO I-Mefs, we clearly observed in KO cells a strong mitochondrial fragmentation (Fig. 4A), which was not evident in the small cytosol of ETNA cells (data not shown). Dynamin related protein 1 (Drp1) is a GTPase that mediates mitochondrial fission through translocation from microtubules to the mitochondria. Moreover, when phosphorylated at Ser616, Drp1 stimulates mitochondrial fission (Scorrano, 2009; Varadi et al., 2004). By separating the mitochondrial and cytosolic fractions of cells, we found that Drp1 localization at mitochondria in Apaf1-deficient cells is greater than in WT cells, in both I-Mefs and ETNA lines (Fig. 4B,C). We also found that the amount of Drp1 phosphorylated at Ser616 is higher in *Apaf1*-KO I-Mefs and ETNA cells than in WT cells (Fig 4B,C). These experiments confirm that there is more mitochondrial fission in KO cells.

Apaf1 depletion leads to impairment of centrosomal microtubule nucleation

The experiments described so far led us to the conclusion that Apaf1 deficiency makes cells more prone to activate apoptotic signaling and to quickly release cytochrome *c*; however, Apaf1-deficient cells do not undergo apoptosis because their apoptosome cannot be formed (Ferraro et al., 2008). The

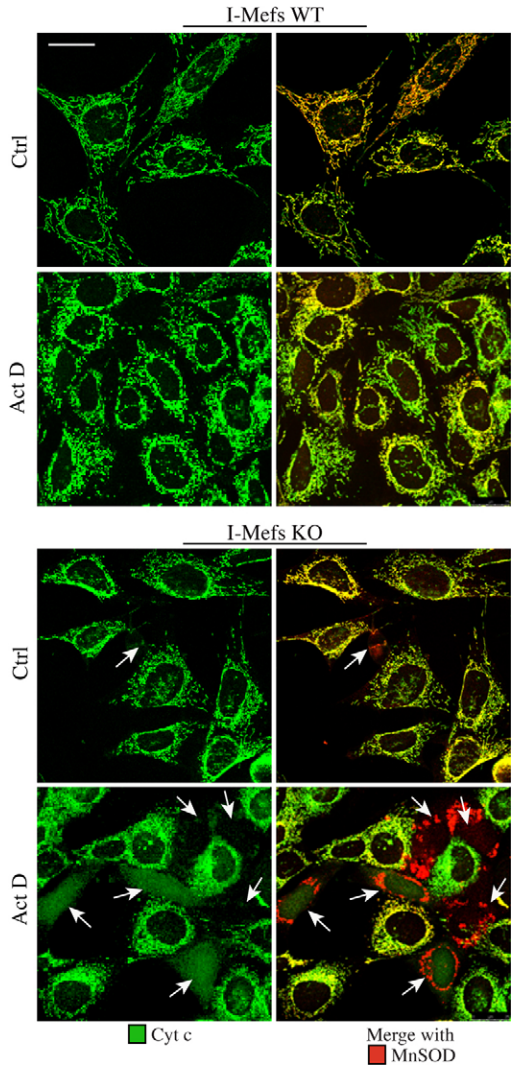

Fig. 2. Faster kinetics of cytochrome *c* release in Apaf1-depleted cells compared with WT cells is not dependent on the kind of apoptotic stimulus applied. Double-labeling immunofluorescence microscopy of I-Mefs WT and I-Mefs KO, not treated (Ctrl) or treated for 20 hours with 10 μM actinomycin D (ActD). Cytochrome *c* staining (green) and the merged images of cytochrome *c* and manganese superoxide dismutase 1 (MnSOD; red), used as marker of mitochondrial localization are shown. White arrows indicate cells with released cytochrome *c*. Scale bar: 25 μm.

increased mitochondrial fission could partly explain the fragility of KO cell mitochondria and the easy release of cytochrome *c* that we observed. The hypothesis is, therefore, that the absence of Apaf1 favors apoptosis initiation and that Apaf1 has an important prosurvival role in the cell other than the apoptotic one.

If this turns out to be the case, Apaf1-deficient cells could show features of fragility, functional impairment or morphological abnormalities. In fact, close examination of Apaf1-deficient cells reveals a number of differences in the shape compared with WT cells. This gross observation and the fact that the cytoskeleton has an important role in regulating mitochondrial network shape (which we found is altered in Apaf1-deficient cells), prompted us to examine cytoskeleton organization. Mitochondria do indeed interact with microfilaments, intermediate filaments and microtubules and, normally, a high proportion (60–70%) of the single mitochondria are located along microtubules (Varadi et al., 2004). We stained actin stress fibers with phalloidin and microtubules with an anti-β-tubulin antibody. No apparent differences in actin cytoskeletal architecture were found between WT and *Apaf1*$^{-/-}$ cells (Fig. 5A). By contrast, the distribution of the tubulin network showed significant aberrations in Apaf1-deficient cells (Fig. 5B): whereas in control cells microtubules originate predominantly from the centrosomes, forming a radial network, in Apaf1-depleted cells the majority of microtubules appeared disorganized and nucleation did not originate from a single centrosomal aster-shaped focus (Fig. 5B). Apaf1 deficiency causes defects in the organization of the microtubule cytoskeleton in primary Mefs also, but the effect is milder than in immortalized cells (data not shown).

To clearly assess whether the absence of Apaf1 cells causes defects in centrosomal microtubule nucleation, we perfomed a microtubule re-growth assay after cold depolymerization. This experiment confirmed that, in Apaf1-deficient cells, microtubules nucleation from the centrosome is impaired and that centrosome asters are not visible, although the formation of cytoplasmic microtubules is not affected and microtubule density is similar to that in controls (Fig. 5C). By contrast, in WT cells, microtubules have a radial, centrosome-based organization and microtubule asters appear very well defined in most cells (Fig. 5C). The results obtained with ETNA cells were similar (data not shown).

Taken together, these results suggest that Apaf1 might have a role in regulating centrosomal microtubule nucleation.

Efficient centrosome and mitotic spindle formation requires Apaf1

Given the impaired microtubule nucleation observed in Apaf1-deficient cells, we analyzed the centrosome components and we found that in both *Apaf1*$^{-/-}$ I-Mef and ETNA cells, there was less centrosome-bound γ-tubulin staining than in WT cells (Fig. 6A,B,E). This indicates that Apaf1 plays a role in centrosome maturation. In addition to the centrosomal γ-tubulin staining observed using immunofluorescence, we also measured the amount of total γ-tubulin by western blot analysis of cell lysates; we observed that the overall amount of the protein was similar in *Apaf1*$^{-/-}$ cells compared with WT cells (data not shown). This means that the depletion of Apaf1 affects only the recruitment of γ-tubulin to centrosomes.

Because centrosomes are the main MTOC of cells and because spindle formation and mitosis depend on them, we decided to analyze mitotic spindle formation in Apaf1-deficient cells. We stained the mitotic spindle with an anti-β-tubulin antibody and visualized DNA with DAPI or with an anti-phosphorylated histone H3 (P-H3) antibody. We found that most of the WT cells had normal mitotic bipolar spindles with aligned DNA in the metaphase plate. By contrast, most KO cells had an abnormal phenotype with disorganized spindles: bipolar spindle with misaligned DNA or multipolar or monocentric spindle (Fig. 6C–F).

We also analyzed mitosis by videorecording the cells and we observed that whereas WT I-Mef cells have a highly regular shape during mitosis, KO I-Mefs have longer mitoses and a deformed morphology, in particular during metaphase and anaphase (Fig. 7A). We observed a similar phenomenon in ETNA cells (Fig. 7B). More specifically, we measured the length of metaphase and anaphase, when the role of the spindle is

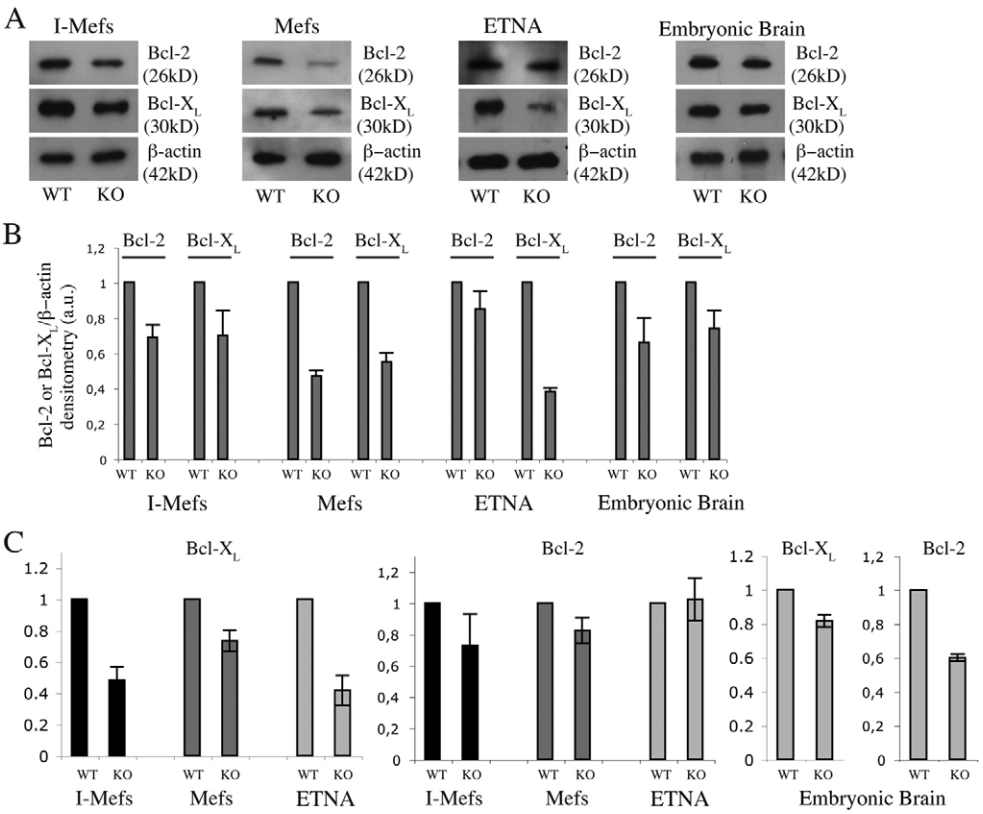

Fig. 3. Apaf1-deficient cells exhibit a low expression of the anti-apoptotic factors Bcl-2 and Bcl-X$_L$. (**A**) Western blot analysis of Bcl-2 and Bcl-X$_L$ expression in total cell lysates of wild type (WT) and knockout (KO) immortalized Mefs (I-Mefs), primary Mefs (Mefs), ETNA (ETNA) cells and E14.5 embryonic brains (Embryonic Brain). β-Actin was also assayed as a control of equal protein loading. (**B**) Densitometric analyses were performed using the software AlphaEaseFC (Alpha-Innotech), normalized for β-actin and reported as arbitrary units (a.u.). Values are means ± s.e.m. of the densitometric analysis of three independent immunoblots. (**C**) The mRNA levels of Bcl-X$_L$ or Bcl-2 were evaluated by quantitative real-time PCR and were normalized to β-actin, used as an internal control. Values are the fold changes (means ± s.e.m.; $n=3$) of Bcl-X$_L$ or Bcl-2 mRNA relative to control cells, which was arbitrarily set as 1.

clearly relevant, and we found that this stage of mitosis lasts, on average, 18.5 and 28 minutes in WT and KO I-Mefs, respectively, and 26 and 36 minutes in WT and ETNA KO cells, respectively (Fig. 7A,B). We can conclude that, in the absence of Apaf1, cells are still able to enter mitosis but with a lower efficiency of correct mitotic division compared with WT

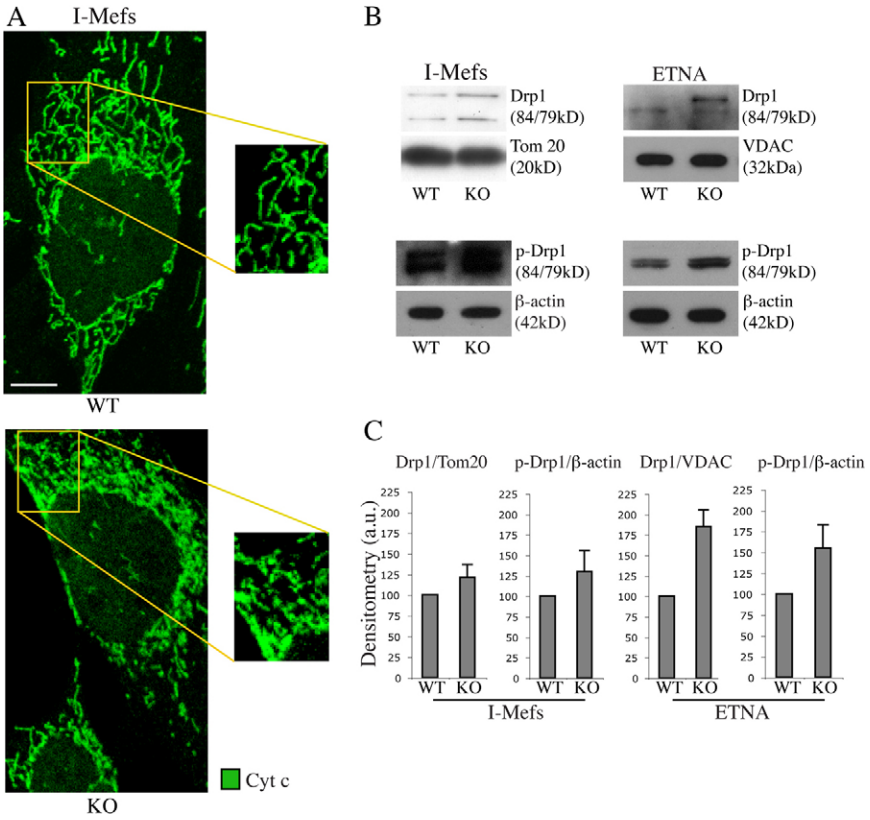

Fig. 4. Mitochondrial fragmentation is increased in Apaf1-depleted cells. (**A**) Immunofluorescence staining of cytochrome *c* (green) to reveal mitochondrial morphology in WT and *Apaf1*-KO I-Mefs. Scale bar: 5 μm. (**B**) *Apaf1*-KO and WT I-Mefs and ETNA mitochondria fractions and total extracts were subjected to SDS-PAGE and analyzed for Drp1 and phosphorylated Drp1 (p-Drp1; at Ser616) protein levels, respectively. Tom20 or VDAC and β-actin were assayed as loading controls in mitochondrial and total extracts. (**C**) Densitometric analyses of immunoblots shown in B were calculated using the software AlphaEaseFC, normalized for Tom20 or for VDAC (mitochondrial markers) or for β-actin and are reported as arbitrary units (a.u.). Values are means ± s.e.m. of the densitometric analysis of four independent immunoblots.

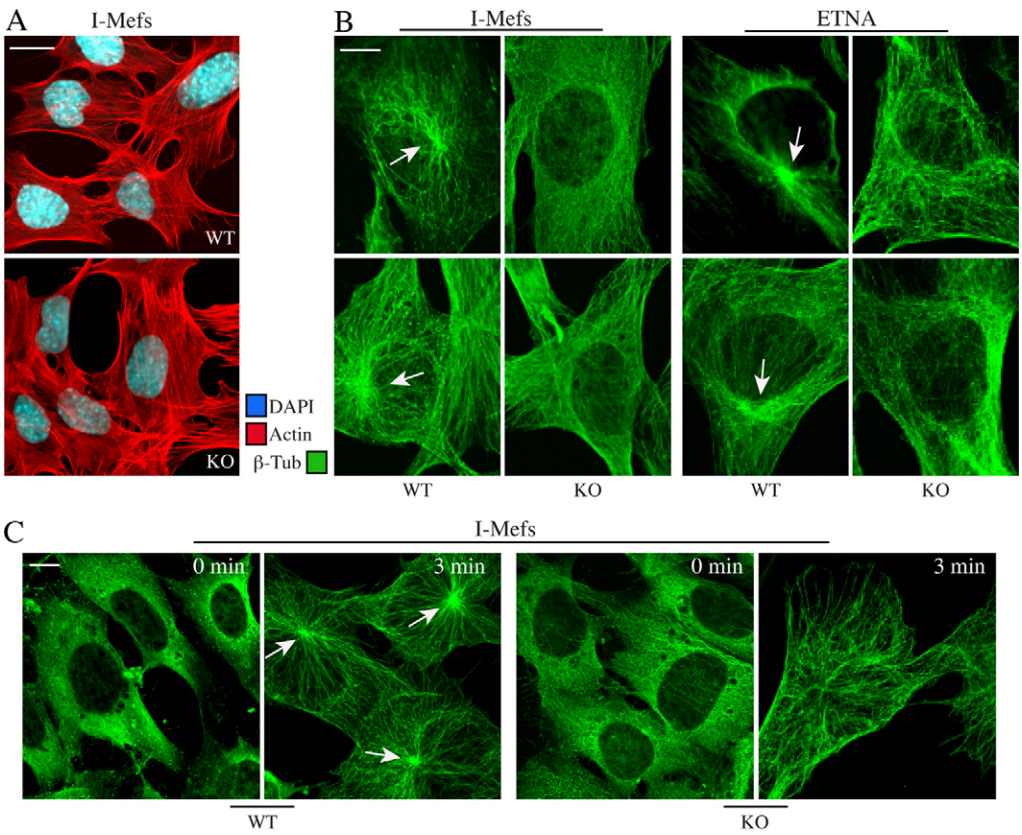

Fig. 5. Centrosomal microtubule nucleation is impaired in Apaf1-deficient cells. (**A**) Staining of I-Mefs to visualize F-actin using TRITC–phalloidin (red). Nuclei were stained with DAPI (blue). Scale bar: 20 μm. (**B**) Immunofluorescence staining of microtubules in I-Mefs and ETNA cells with an anti-β-tubulin antibody (green). Arrows indicate microtubule asters (WT). Asters are barely visible in Apaf1-deficient cells (KO). Scale bar: 10 μm. (**C**) Microtubule regrowth assay in I-Mefs. Cells were cold treated for 1 hour to achieve depolymerization of microtubules, then they were re-heated for 0 or 3 minutes at 37°C to allow microtubules re-growth. Cells were then fixed and the microtubules stained with an anti-β-tubulin antibody (green). Scale bar: 5 μm.

cells, as featured by the longer time to complete mitosis and the irregular shape of dividing cells (Fig. 7A,B). From these data, we also observed that *Apaf1*-KO cells proliferate more slowly than WT cells.

The mitotic spindle is essential for accurate chromosome segregation, and centrosome abnormalities are often associated with chromosomal instability. In some cases, centrosomal impairment can lead to aberrant mitosis that is unable to undergo completion thanks to checkpoints that trigger cell death. Indeed, although Apaf1-depleted cells do not undergo apoptosis, some cells die by other types of cell death, as shown by propidium iodide staining in conditions of Apaf1 deficiency (Fig. 7C, subG1). In other cases, although cytokinesis occurs and daughter cells are viable, these suffer severe aneuploidy or fail cytokinesis and continue to cycle, becoming large multinucleated polyploid cells with supernumerary centrosomes, as we found in ETNA KO cells (supplementary material Fig. S1).

Apaf1-deficient cells are defective in cell migration

Because centrosomes and microtubule assembly and dynamics are also important for cell motility (Kodani and Sutterlin, 2008; Watanabe et al., 2005), we also analyzed cell migration in Apaf1-depleted cells. We performed a wound-healing assay and we observed that, after 20 hours, WT I-Mefs had almost filled the wound made by a scratch between cells. By contrast, KO cells were much slower to migrate into the wound (Fig. 8A,B). In particular, even though we observed a movement of Apaf1-depleted cells toward the wound soon after the scratch, they subsequently slowed down, showing a trend to interact laterally with the other cells in order to first completely fill the space between cells and, only later, migrating toward the wound (Fig. 8A). Moreover, immunofluorescence of γ-tubulin 30 minutes after the scratch indicated that there were fewer Apaf1-deficient I-Mefs than WT cells with centrosomes oriented toward the wound edge (Fig. 8C). Thus, on the basis of these results, it can be concluded that Apaf1 influences cell migration most probably through its effects on centrosomes and on microtubule assembly and dynamics.

Apaf1 absence reduces the recruitment of HCA66 and other centrosomal proteins to centrosomes

One possible explanation of the role of Apaf1 in regulating centrosomal stability, which is needed for cell division and motility, is that Apaf1 might interact with centrosomal proteins. Strikingly, one of the known Apaf1 interactors, HCA66, has been found very recently to be localized into centrosomes (Fant et al., 2009).

Therefore, we examined whether Apaf1 depletion could affect the localization of HCA66. By immunofluorescence assays of WT I-Mefs, we found that HCA66 was highly dispersed in the cytosol and that its localization to centrosomes was affected in Apaf1-deficient cells (Fig. 9A,B). The same result was found in ETNA cells (data not shown).

We then analyzed the effect of Apaf1 deficiency on HCA66 protein levels and found, surprisingly, that HCA66 increased in I-Mefs (Fig. 9C) and also in ETNA cells (data not shown). In sum, we observed that, in the absence of Apaf1, there was an increased expression of HCA66, which was associated with its decreased centrosomal localization. Because centrosomes are intimately connected with the nuclear envelope, we decided to test the association of HCA66 with the nuclear envelope in WT and Apaf1-deficient I-Mefs at the biochemical level. To this aim, we isolated nuclei of I-Mefs by nuclear–cytosolic fractionation. The

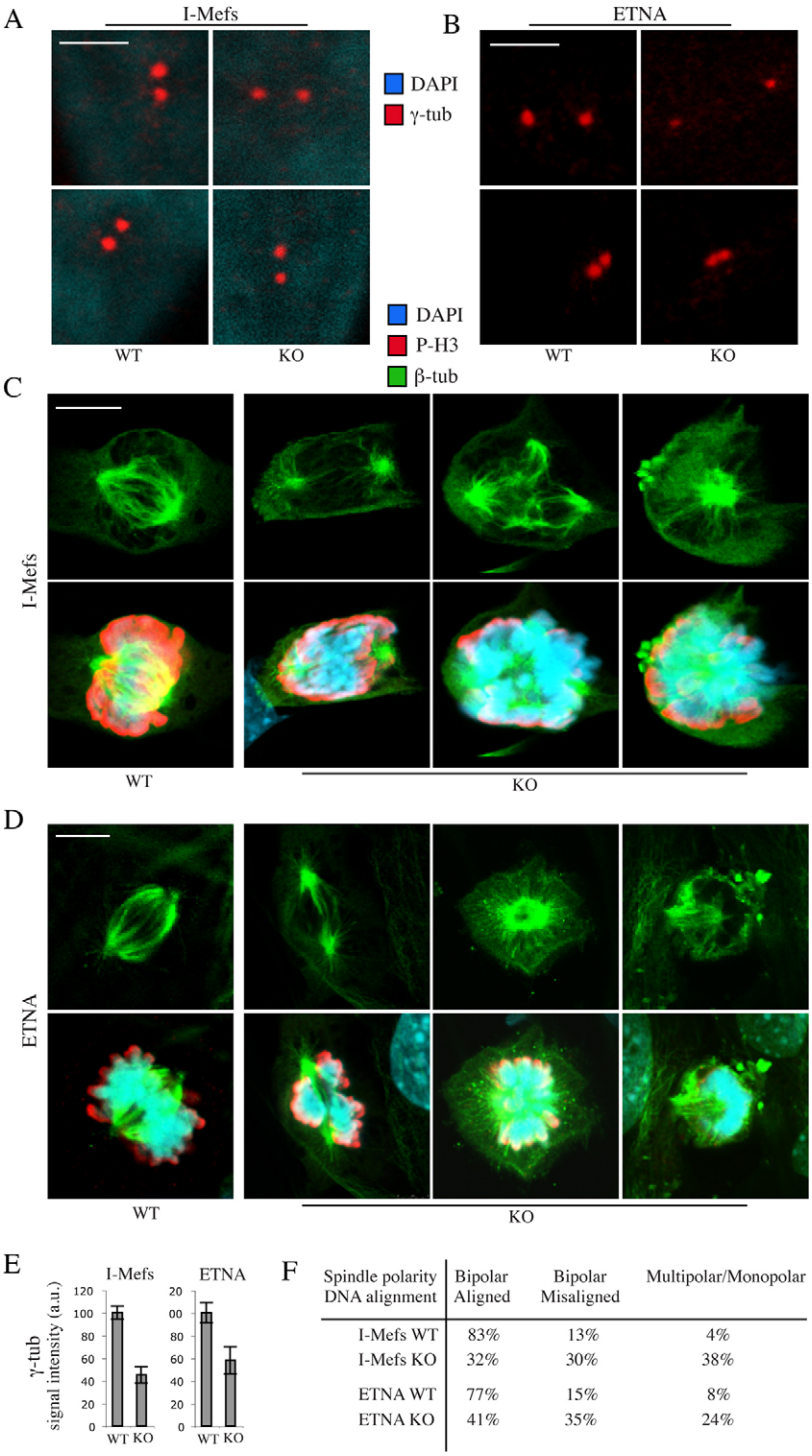

Spindle polarity DNA alignment	Bipolar Aligned	Bipolar Misaligned	Multipolar/Monopolar
I-Mefs WT	83%	13%	4%
I-Mefs KO	32%	30%	38%
ETNA WT	77%	15%	8%
ETNA KO	41%	35%	24%

Fig. 6. Efficient centrosome and mitotic spindle formation requires Apaf1. (**A**) Immunofluorescence staining of γ-tubulin (red) and DAPI staining in WT and KO I-Mefs. Scale bar: 5 μm. (**B**) Immunofluorescence staining of γ-tubulin (red) in WT and KO ETNA cells. Scale bar: 5 μm. (**C**) I-Mefs and (**D**) ETNA cells were stained with anti-β-tubulin antibody (green) to monitor the microtubule organization, with an anti-phosphorylated histone H3 antibody (red), and DAPI dye (blue) to visualize DNA. Scale bar: 10 μm. Spindle organization and DNA alignment were used as criteria to define the mitotic phenotype. (**E**) ImageJ quantitative analysis of the intensity of γ-tubulin immunofluorescence at the centrosomes shown in A and B. At least 60 centrosomes were analyzed for each cell type in two independent experiments. Values are means ± s.e.m. for both WT and KO cells. (F) Quantification of the spindle phenotype in WT and KO I-Mefs and ETNA cells (n=3).

nuclei-containing pellets were extracted with detergents at low salt concentration (1% Triton X-100), the extracts were centrifuged and supernatants (S) and pellets (P) were analyzed by western blotting (Padmakumar et al., 2005) to determine the distribution of HCA66 (Fig. 9D). The distribution of the well-characterized inner nuclear envelope protein lamin A/C served as a control. We observed that, under the conditions used, lamin A/C is completely resistant to extraction (Fig. 9D, lanes P). Resistance to solubilization and presence in the pellet indicates that a protein is an integral membrane protein with a tight interaction with lamina A/C. Centrosomal proteins are bound to the outer nuclear envelope membrane and are easily solubilized by mild extraction conditions. Indeed, γ-tubulin (used as a marker of the centrosomes) is found in both the pellet and the soluble fraction, and HCA66 has the same distribution. Interestingly, in Apaf1-deficient cells, soluble HCA66 is more abundant than in WT cells, whereas the pellet fraction is similar in the two genotypes, meaning that, in Apaf1-depleted cells, HCA66 (although more expressed) is more loosely bound to the nuclear envelope than it is in WT cells (Fig. 9D). We found the

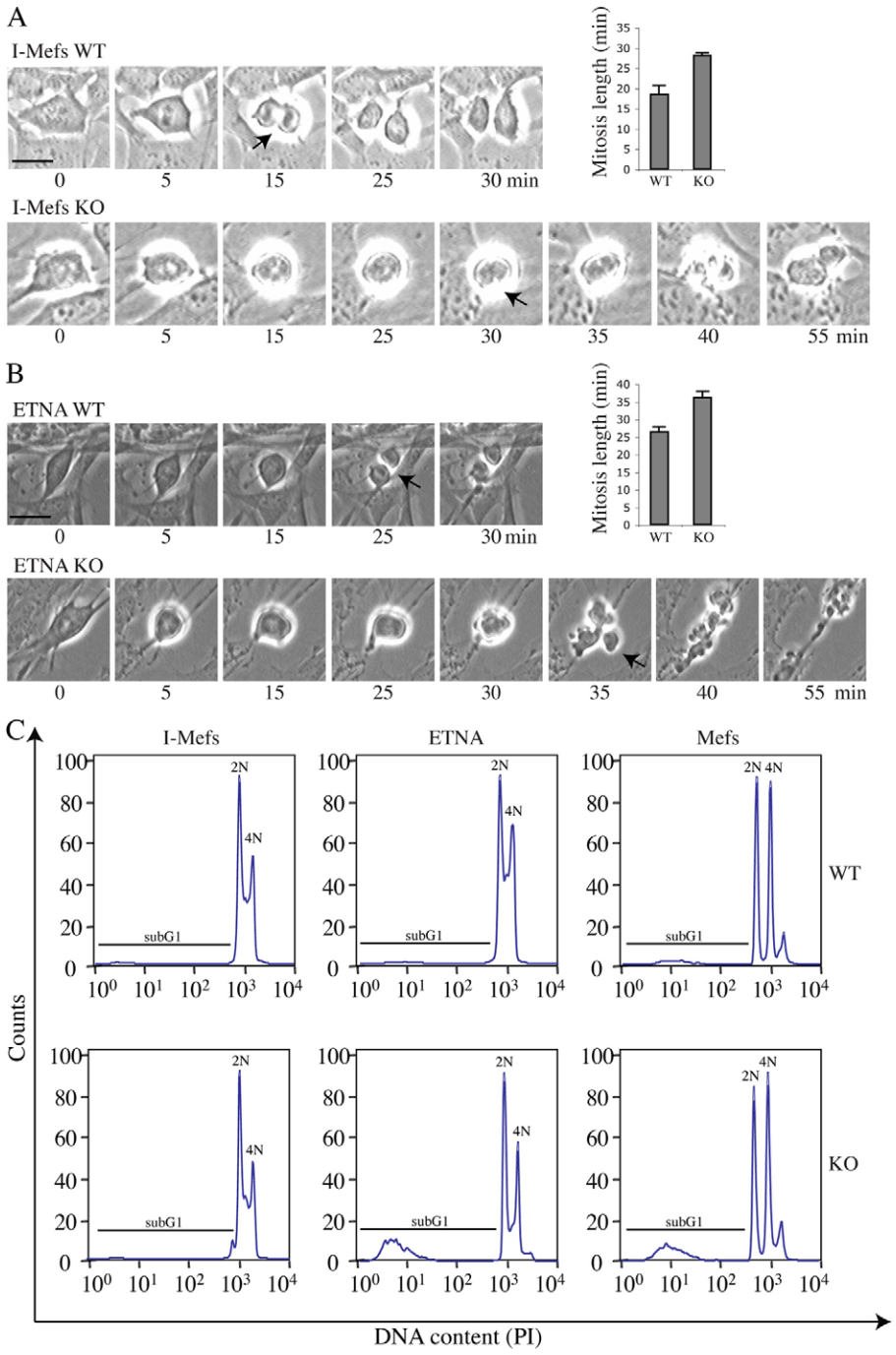

Fig. 7. Apaf1-deficient cells have longer mitosis and increased basal non-apoptotic cell death. (**A**,**B**) Time-lapse analysis of dividing WT and KO I-Mefs (A) or WT and KO ETNA cells (B) was performed and one representative example for each cell line is reported. The length of mitosis was measured starting from the very early detachment of the cell from the dish until the appearance of the two new cells (arrow). The corresponding histograms show the calculated duration of mitosis for each cell line. Values are means ± s.e.m. of 30 mitotic cells for each cell line. Scale bar: 20 μm. (**C**) DNA content of cells as determined by propidium iodide staining of the indicated cell lines in the absence of toxic stimuli. Besides the G1 phase (2N) and the G2–M phase (4N) cells, note the subG1 population indicative of dead cells. The data are representative of three separate experiments.

same results in ETNA cells (Fig. 9D), and also by using more stringent extraction conditions (1% Triton X-100, 250 mM NaCl; data not shown). Notably, in the pellet fraction, HCA66 has a faster electrophoretic mobility compared with the HCA66 in the soluble fraction.

Also, we evaluated the amount of other centrosomal proteins and we observed that the centrosomal localization of NEDD1, ninein and Cep192 was reduced in both Apaf1-deficient cell lines (Fig. 9E,F, and data not shown), whereas pericentrin and PCM-1 appeared unaffected. To prove that the centrosome impairment found in *Apaf1*-KO cells can also affect cytochrome *c* release, we performed RNA silencing of NEDD1 in WT I-Mefs (supplementary material Fig. S2). We observed that the partial depletion of NEDD1 enhances cytochrome *c* release under tunicamycin treatment (supplementary material Fig. S2C).

Taken together, these analyses suggest that Apaf1 might exert its role in regulating centrosomal stability and the localization of a number of centrosomal proteins through its effect on HCA66 localization.

When overexpressed, Apaf1 localizes to the outer nuclear envelope

In order to explain how Apaf1 regulates the recruitment of HCA66 to centrosomes, we hypothesized that Apaf1 might

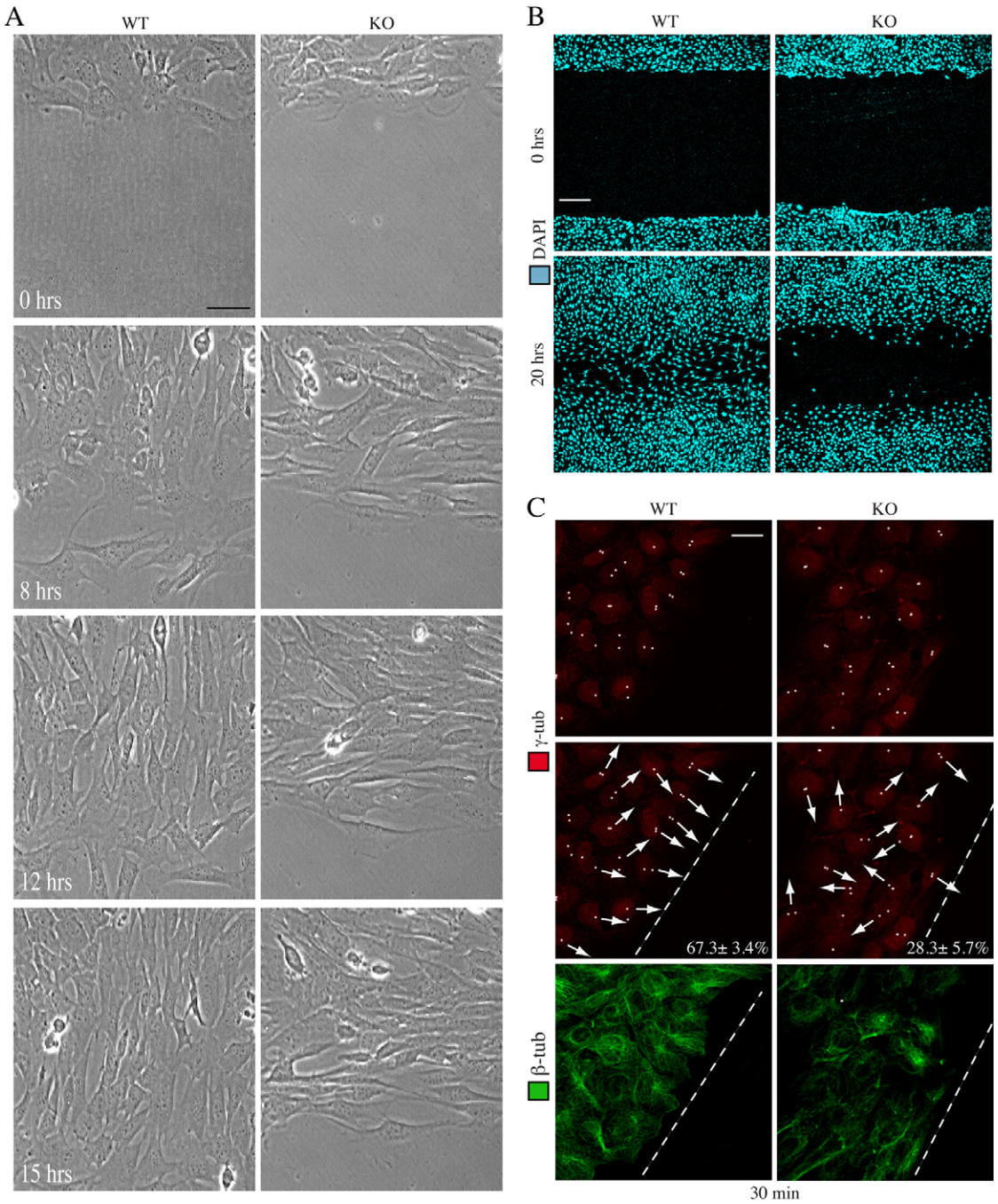

Fig. 8. Cell migration and centrosome re-orientation in wound healing assays. (**A**) Migration of WT and KO I-Mefs into a scratch wound was monitored by live-cell imaging. Scale bar: 50 μm. (**B**) Cells were fixed and stained with DAPI soon after the scratch and after 15 hours to evaluate the migration ability of Apaf1-depleted I-Mefs into the wound. Scale bar: 300 μm. (**C**) In order to analyze centrosome re-orientation (arrows) towards a scratch wound, I-Mefs were fixed and stained with anti-γ-tubulin and anti-β-tubulin 30 minutes after introduction of the scratch wound. Centrosomes have been marked with white dots to highlight their position. The white dashed line indicates the scratch direction. The percentage of cells with centrosomes that are directed toward the wound edge 30 minutes after introduction of the scratch wound is indicated at the bottom right. 200 cells of either cell type were analyzed. Scale bar: 25 μm.

localize to the centrosomes, interacting with HCA66. Therefore, we performed an immunofluorescence analysis of overexpressed Apaf1 (because the endogenous one is universally recognized as undetectable by this technique), but we did not find any centrosomal localization of this protein. Very interestingly, however, we found overexpressed Apaf1 to be highly localized on the outer nuclear envelope and ER, showing a pattern very similar to that of the ER marker protein disulfide isomerase (PDI; Fig. 10A–C). As a negative control, we overexpressed an unrelated protein that does not have a nuclear envelope or ER localization (superoxide dismutase 1; SOD1), and we performed exactly the same procedure used for Apaf1 detection (Fig. 10B). The specificity of the Apaf1 localization assay was also confirmed by the fact that upon simultaneous exogenous Apaf1

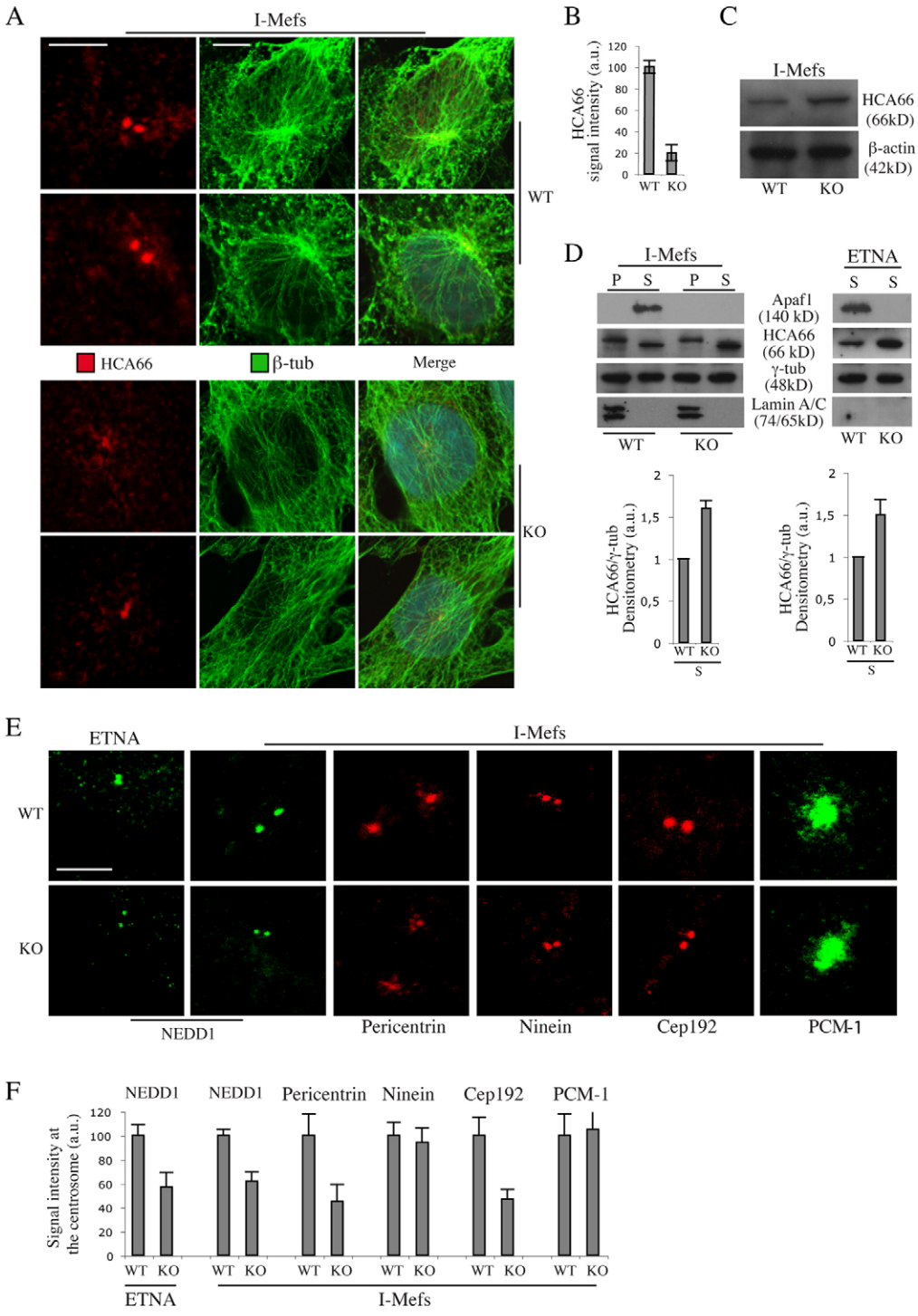

Fig. 9. Apaf1 deficiency reduces HCA66 and other centrosomal protein recruitment to centrosomes. (**A**) Immunofluorescence staining of HCA66 (red) and β-tubulin (green) in WT and KO I-Mefs (two representative images for each genotype are shown). Merged images of the two staining is also shown. Scale bar: 5 µm. (**B**) Quantitative analysis of the intensity of HCA66 immunofluorescence at the centrosomes (using ImageJ). At least 60 centrosomes were analyzed for each genotype in several images collected in two independent experiments. Values are means ± s.e.m. (**C**) Western blot analysis of HCA66 expression in total I-Mef lysates. β-actin was assayed as loading control. (**D**) Solubilization properties of HCA66 in WT and KO cells. Purified nuclei of I-Mefs and ETNA cells were isolated by nuclear–cytosolic fractionation and were then extracted in the same buffer containing 1% Triton X-100. The extracts were centrifuged and supernatants (S) and pellets (P) were analyzed by western blotting to determine the location of HCA66. Lamin A/C was used as a control for the location of the inner nuclear envelope, and γ-tubulin as a centrosome marker. Immunoblots are from one experiment representative of three that gave similar results. Cell densities were calculated using the software AlphaEaseFC, normalized for γ-tubulin and reported as arbitrary units (a.u.). Values are means ± s.e.m. of three independent immunoblots. (**E**) Immunofluorescence staining of NEDD1, PCM-1 (green), pericentrin, ninein and Cep192 (red) in WT and KO I-Mefs. NEDD1 was also analyzed in ETNA cells. Scale bar: 5 µm. (**F**) Quantitative analysis of the intensity of NEDD1, PCM-1, pericentrin, ninein and Cep192 immunofluorescence at the centrosomes was performed using ImageJ software. At least 60 centrosomes were analyzed for each marker in several collected images. Values are means ± s.e.m.

transfection, small interfering RNA (siRNA) for Apaf1 strongly reduces the expression of Apaf1 (supplementary material Fig. S3). If Apaf1 plays a role in the nuclear envelope structure, nuclear morphology could be altered in *Apaf1*-KO cells. Indeed, we observed that nuclei in Apaf1-deficient cells are larger (Fig. 10D, length and breadth) and that the DAPI signal intensity (represented by the average gray factor) is lower, suggesting that the chromatin packing is loose in this context. This difference was also detected in ETNA cells (data not shown). Interestingly, upon reintroduction of Apaf1 by transfection, we observed a recovery of the normal nuclear size and DAPI intensity (Fig. 10D, KO+Apaf1).

Discussion

Besides mitochondrial cell death regulation, Apaf1 has other functions not related to apoptosis, which, upon DNA damage, cause cell cycle arrest and DNA damage checkpoints (Zermati et al., 2007). Here we show that Apaf1 also plays a role in normal conditions (i.e. unrelated to its pro-apoptotic role) and not only upon DNA damage induction or other stress stimuli. We have

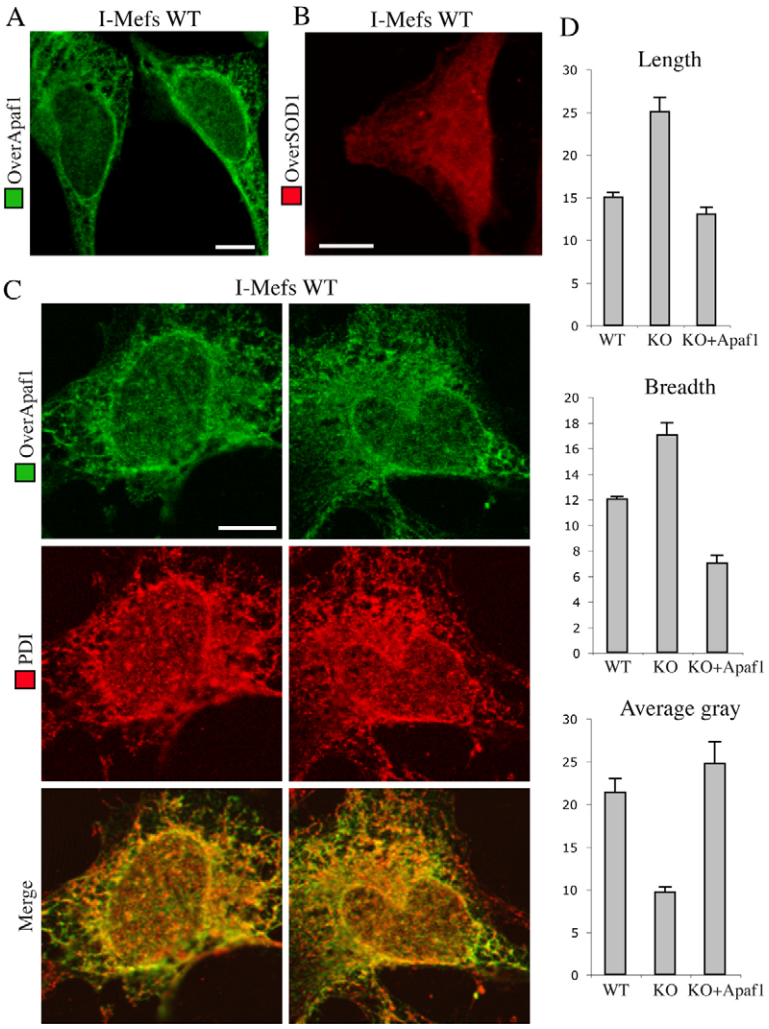

Fig. 10. Overexpressed Apaf1 is partially located on the outer nuclear envelope and on the ER and restores the normal nuclear size. (**A**) Immunofluorescence detection of overexpressed Apaf1 (green) in WT I-Mefs. (**B**) Immunofluorescence detection of overexpressed SOD1 (red) in WT I-Mefs. (**C**) Immunofluorescence detection of overexpressed Apaf1 (green) and PDI (red), and merged images of both, in WT I-Mefs. Two representative images are shown. Scale bar: 10 μm. (**D**) Analysis of nuclei size in I-Mefs; length, breadth and average gray of nuclei of WT cells, *Apaf1*-KO cells and *Apaf1*-KO cells overexpressing Apaf1 were measured using Metamorph software. The average gray is a measure of the DAPI signal intensity. For each experimental condition, at least 52 cells were analyzed and data are presented as means ± s.e.m. According to Student's *t*-test, all results are statistically significant.

found that the absence of Apaf1 impairs centrosome stability and affects basic cellular processes such as spindle formation, mitosis, mitochondrial morphology (the impairment of which has been reported to increase the responsiveness of cells to stress) and cell migration, thus causing the higher fragility of Apaf1-deficient cells compared with WT cells.

In the first part of the paper we have shown that Apaf1 deficiency induces a lower expression of the anti-apoptotic proteins Bcl-2 and Bcl-X_L, which contributes to explaining (together with the high degree of mitochondrial fission we observed) the ease with which Apaf1-deficient cells release cytochrome *c* (Figs 1–3). Low levels of Bcl-2 and Bcl-X_L increase permeabilization of mitochondria, leading to a lower threshold in the stress response and a higher fragility of Apaf1-deficient cells compared with WT cells. However, they do not enhance apoptosis, because Apaf1 depletion impairs apoptosis. Therefore, upon strong toxic insults, even though *Apaf1*-KO cells are faster in responding to the insults and in initiating the apoptotic pathway, they do not die, unlike WT cells. Sublethal insults for WT cells might turn out to be sufficient to stimulate the first stages of the apoptotic signaling in KO cells, because they are more sensitive to stress. However, despite the fact that *Apaf1*-KO cells do not complete apoptosis, over time, if the toxic stimulus is continuous, a combination of Drp1-dependent fragmented mitochondria, low levels of anti-apoptotic proteins, fast cytochrome *c* release and aberrant mitosis (characterizing Apaf1-deficient cells) could ultimately induce other forms of cell death and, under conditions that are sublethal for WT cells, *Apaf1*-KO cells will paradoxically show higher cell death than WT cells do (Fig. 7C).

We set out to investigate the reasons for Apaf1-deficient cell fragility and we found that the prosurvival role of Apaf1 could be due, at least in part, to its effect on centrosome stability and microtubule nucleation, which affect mitochondrial network shape, spindle formation and mitosis (Figs 4–7). Moreover, it is known that spindle aberrations can cause chromosome instability (Fukasawa, 2007). In fact, among $ETNA^{-/-}$ cells we have observed a substantial number of multinucleated cells with several centrosomes and an increased number of micronuclei, which suggests chromosome segregation defects (see supplementary material Fig. S1). Gain or loss of chromosomes greatly accelerates tumor progression (Fukasawa, 2007), and it has been suggested that the correlation between Apaf1 deficiency and cancer might be not only due to the absence of apoptosis but also to the absence of checkpoints (Zermati et al., 2007). In addition, we propose that this effect might also be related to the chromosome instability caused by microtubule and spindle defects.

We wanted to unravel how Apaf1 acts on centrosomes. We discovered that, in the absence of Apaf1, recruitment of HCA66 to the centrosome is reduced (Fig. 9A,B,D); such a reduction has previously been reported as causing disorganized microtubule nucleation from centrosomes (Fant et al., 2009). Because HCA66 is an Apaf1 interactor, the lack of their binding might account for the dysregulation of HCA66 centrosomal localization we observed in the absence of Apaf1. Interestingly, the phenotype we describe in *Apaf1*-KO cells is very similar, although milder, to that reported for HCA66 KO cells, which includes spindle microtubule assembly defects (Fant et al., 2009). The higher levels of HCA66 in Apaf1-deficient cells (Fig. 9C) might be a response of the cell aimed at counteracting the poor centrosomal localization of HCA66.

We also found that the *Apaf1*-KO phenotype shows a striking similarity to the knockout phenotype of the Golgi protein GM130 (Kodani and Sutterlin, 2008). On the basis of this phenotype (which includes aberrant spindle formation, centrosome dysmorphology and defective microtubule organization and cell migration), this protein has been defined as a regulator of centrosome morphology and function.

The effect of Apaf1 absence on HCA66 centrosomal localization would be easily explained if Apaf1 had localized to the centrosomes. However, we could not observe a centrosomal localization of overexpressed Apaf1 (Fig. 10A,C). Of note, overexpressed HCA66 was also not detectable within the centrosomes (data not shown), whereas endogenous HCA66 was clearly centrosomal (see Fig 9A); therefore, we cannot rule out a centrosomal localization of endogenous Apaf1. Very interestingly, when we overexpressed Apaf1 in cells, besides a diffuse presence into the cytosol, we also detected a clear localization of this protein to the ER and also to the ER region forming the outer layer of the nuclear envelope (Fig. 10A,C). Indeed, although most studies continue to report Apaf1 as being diffuse into the cytosol (Hausmann et al., 2000; Wang, 2001), some show a perinuclear and Golgi localization of Apaf1 (Ruiz-Vela et al., 2001) or its localization in membrane domains at or near the plasma membrane (Sun et al., 2005). There have also been other reports of nuclear accumulation of Apaf1 and perinuclear accumulation of its nematode ortholog CED-4 (*Caenorhabditis elegans* death-promoting protein-4) upon DNA damage (Besse et al., 2004; Ruiz-Vela et al., 2002; Zermati et al., 2007).

Because it is known that centrosomes are intimately connected with the nuclear envelope (reviewed by Gonczy, 2004), and that proteins from the outer nuclear envelope regulate the composition of the centrosome (Malone et al., 2003; Salpingidou et al., 2007), the localization of overexpressed Apaf1 at the outer envelope suggests that it might interact there with HCA66, and favor the recruitment of HCA66 to the centrosomes. We observed that, upon nuclear extraction, HCA66 in the nuclear soluble fraction (Fig. 9D) has a lower molecular mass than that isolated from the pellet (Fig. 9D), an effect that is most probably due to a post-translational modification. Because the low molecular mass HCA66, which weakly bound to the nucleus, is more abundant in conditions of Apaf1 deficiency (Fig. 9D), we speculate that, in the absence of Apaf1, HCA66 is not efficiently modified and, in turn, it might have more difficulty in being recruited to the centrosomes or, vice versa, it is less efficiently recruited to centrosomes and thus less efficiently modified.

The outer membrane localization of Apaf1 might also have a structural role on the nuclear envelope, which becomes loose in its absence, so influencing nuclear size; in fact, Apaf1-deficient nuclei are larger and chromatin is more loosely packaged (Fig. 10D). This might be another explanation for the weakness of Apaf1-deficient cells, because nuclei might be more sensitive to physical stress.

To sum up, we report here a novel prosurvival role for Apaf1, which we showed to be partly localized at the ER and outer nuclear envelope. We discovered that Apaf1, through its binding and regulation of HCA66 centrosomal localization, participates in regulating centrosomal microtubule nucleation and therefore also spindle assembly, cell migration and mitochondrial network organization. Although the exact molecular mechanism of this regulation needs to be understood in more depth, this finding suggests challenging new scenarios regarding the regulation of the equilibrium between cell death and survival.

Materials and Methods

Plasmid constructs

Apaf1 expression plasmid was created by PCR cloning of murine Apaf1 cDNA (Cecconi et al., 1998) from the plasmid described previously (Cozzolino et al., 2004) between the *Apa*I and *Not*I sites of pShuttle (Clontech). SOD1 expression plasmid was described elsewhere (Cozzolino et al., 2004).

Cell cultures and treatments

ETNA wild-type and ETNA$^{-/-}$ cells were obtained as described elsewhere (Cozzolino et al., 2004). They were routinely grown in DMEM (Gibco BRL) + 10% FBS (Gibco BRL), at 33℃ in an atmosphere of 5% CO_2 in air. Mouse embryonic fibroblasts (Mefs) were manually dissected from wild-type and homozygous E13.5 embryos and cultured in DMEM supplemented with 10% FBS at 37℃. Mefs were immortalized with SV40 antigen. ETNA cells stably expressing dominant negative caspase-9 (C9DN-ETNA) were obtained as described previously (Ferraro et al., 2008). To induce apoptosis, I-Mefs were treated with 2 μg/ml tunicamycin or 10 μM actinomycin D for 20 hours. ETNA cells were treated with 20 μM actinomycin D or 3 μg/ml tunicamycin for 24 hours, then MG132 (2 μM) was added for a further 40 hours.

Immunocytochemistry

Cells cultured in 35-mm Petri dishes were washed in PBS and fixed with methanol–acetone at –20℃ for 10 minutes or with 4% PFA in PBS for 15 minutes. After permeabilization with 0.4% Triton X-100 in PBS for 5 minutes (performed only after PFA fixation), cells were blocked in 2% horse serum in PBS and incubated for 1 hour at 37℃ with primary antibodies. The following antibodies were used: anti-cytochrome *c* (clone 6H2.B4; Assay Designs), anti-β-tubulin (Sigma-Aldrich), anti-NEDD1 (Abcam) monoclonal antibodies and anti-MnSOD1 (Stressgen), anti-Apaf1 (BD Transduction Laboratories), anti-PDI (Stressgen), anti-γ-tubulin (Sigma-Aldrich), anti-HCA66, anti-ninein, anti-PCM-1 (three kind gifts from A. Merdes, CNRS-Pierrre-Fabre, Toulouse, France), anti-pericentrin (a kind gift from T. Davis, University of Washington, Seattle, WA) anti-Cep-192 (a kind gift from L. Pelletier, University of Toronto, Toronto, ON, Canada) and anti-phosphohistone H3 (Upstate) polyclonal antibodies. Cells were then washed in blocking buffer and incubated for 1 hour with labeled anti-mouse (Alexa Fluor 488 or Alexa Fluor 555; Molecular Probes) or anti-rabbit (FITC or Cy3; Jackson ImmunoResearch) secondary antibodies. After rinsing in blocking buffer, cell nuclei were stained with 1 mg/ml DAPI and examined under a Leica TCS SP5 confocal microscopy. Fluorescence images were adjusted for brightness, contrast and color balance using Adobe Photoshop CS.

Immunoblotting

After rinsing the cultures with ice-cold PBS, cell lysis was performed in RIPA buffer (20 mM Tris-HCl, pH 7.4, 1% Triton X-100, 150 mM NaCl, 1 mM EDTA, 5 mM $MgCl_2$) containing a protease inhibitor cocktail (Sigma-Aldrich). A clear supernatant was obtained by centrifugation of lysates at 13,000 ***g*** for 10 minutes. Protein content was determined using the Bradford protein assay (Bio-Rad). Western blots were performed on polyvinylidene difluoride membranes (Immobilon P; Millipore). Equal loading of samples was confirmed by β-actin (Sigma-Aldrich) or voltage-dependent anion-selective channel protein (VDAC; Calbiochem) normalization. Polyclonal anti-Bcl-X S/L (S-18), anti-lamin A/C (N-18) and anti-Tom20 (FL-145) antibodies were purchased from Santa Cruz Biotechnology. To detect Drp1, a monoclonal antibody (anti-Dlp1, clone 8) from BD Biosciences or from Cell Signaling and a polyclonal antibody anti-phospho-Drp1 (Ser 616) from Cell Signaling were used.

Monoclonal antibodies, anti-Apaf1 and anti-Bcl2, were purchased from BD Biosciences and Santa Cruz Biotechnology, respectively. A polyclonal antibody, anti-γ-tubulin, was purchased from Sigma-Aldrich and a polyclonal antibody, anti-HCA66, was a kind gift form A. Merdes (CNRS-Pierrre-Fabre, Toulouse, France).

Real-time RT-PCR

RNA was isolated using an RNeasy Micro Kit (Qiagen Inc), according to the manufacturer's instructions. For RT-PCR, first strand cDNA was synthesized with esaprimers by adding 1 μg of RNA with M-MLV reverse transcriptase (Invitrogen). Real-time PCR was performed by using SensiMix Plus SYBR Kit (Quantace Ltd). The following primers were used: mouse Bcl-xL forward 5′-GGTGAGTCGGATTGCAAGTT-3′, reverse 5′-AAGAGTGAGCCCAGCAG-AAC-3′; mouse Bcl-2 forward 5′-GTACCTGAACCGGCATCTG-3′, reverse 5′-GGGGCCATATAGTTCCACAA-3′. Real-time quantification was performed by using a Fast Real-Time PCR System (Applied Biosystems). Data were normalized to β-actin (forward 5′-AGCCATGTACGTAGCCATCC-3′, reverse 5′-CTCT-CAGCTGTGGTGGTGAA-3′). Fold change was determined by using the $2^{-\Delta\Delta CT}$ method (Livak and Schmittgen, 2001). All reactions were performed in triplicate.

Time-lapse video microscopy

A Zeiss Axiovert-35 microscope equipped with a JVC digital CCD camera and IAS2000 software (Deltasistemi, Rome, Italy) was used to take images every 5 minutes for an observation period of 20 hours. Applying the 'visualize' mode, these series of photographs were displayed as continuous time-lapse movies. Cells were seeded the day before recording into 35-mm dishes. Temperature was adjusted to 33℃ or 37℃ with a Peltier apparatus. A 50× magnification was applied.

Wound healing assay

Cells were seeded the day before recording as a confluent monolayer onto 35 mm dishes. Scratch wounds were introduced using a pipette tip and medium was changed to remove debris and mitotic cells. Time-lapse video microscopy was then performed to monitor the wound healing.

Microtubule regrowth assay

The medium of cells grown on 35-mm dishes was changed with precooled medium and cells were transferred onto ice for 1 hour and then into prewarmed medium at 37℃. Regrowth was stopped after 3 minutes by methanol–acetone fixation.

Analysis of cell viability

Adherent and detached cells were combined and stained with 50 μg/ml propidium iodide before analysis using a FACScalibur instrument (BD Biosciences). Apoptotic cells were evaluated by calculating peak areas of hypodiploid nuclei in previously premeabilized cells (subG1).

Nuclear–cytosolic fractionation

Cells were detached from the dish with trypsin and washed with PBS. Pellets were incubated in ~5 vol. ice-cold hypotonic buffer (10 mM Hepes pH 7.4, 5 mM $MgCl_2$, 10 mM NaCl, 1 mM DTT) containing a protease inhibitor cocktail (Sigma-Aldrich) and the phosphatase inhibitors Na_3VO_4 (1 mM) and NaF (1 mM), and homogenized in a glass–glass homogenizer (Dounce homogeniser) using 100 strokes of a tight-fitting pestle. The soluble cytoplasmic, and the insoluble nuclear fractions were separated by centrifugation at 2000 ***g*** for 10 minutes at 4℃. The pellets containing the nuclei were extracted in the same buffer containing either 1% Triton X-100 or 1% Triton X-100 and 250 mM NaCl. The extracts were centrifuged at 15,000 ***g*** for 10 minutes at 4℃ and supernatants and pellets were analyzed by western blotting.

Mitochondrial fractionation

Subcellular fractionation was performed as previously described (Frezza et al., 2007). Briefly cells were harvested with a cell scraper and homogenized with a glass–Teflon potter in isolation buffer (10 mM Tris–Mops, 1 mM EGTA–Tris, 200 mM sucrose). Supernatant was collected after centrifuging at 600 ***g*** for 10 minutes. After centrifuging once more at 7000 ***g*** for 10 minutes the protein concentration of the crude mitochondrial pellet was determined and equal amount of protein were separated by SDS-PAGE.

Transfection procedures

Apaf1 and SOD1 expression plasmids and double-stranded siRNA oligomers were transiently transfected using Lipofectamine2000 according to the manufacturer's instructions (Invitrogen). For Apaf1 and NEDD1 silencing we used the smart pool siRNA directed against four NEDD1 and Apaf1 mRNA sequences specific for mouse (Dharmacon). Their sequences are available on request. Control cells were transfected with a scrambled siRNA duplex (Ambion), which does not show homology with any other murine mRNAs.

Data presentation

All experiments were performed at least three times, unless otherwise indicated. Data are expressed as means ± s.e.m. The significance of differences between populations of data were assessed by Student's *t*-tests and differences with $P \leq 0.05$ were considered as significant.

Acknowledgements

We are grateful to F. Florenzano, V. Frezza and M. T. Ciotti for research assistance, to J. L. Poyet, L. Pelletier, T. Davis and A. Merdes for the gift of reagents.

Funding

This work was supported by grants from the Associazione Italiana per la Ricerca sul Cancro (AIRC) [grant no. IG10081], the Telethon Foundation [grant no. S99038TELC], the Health and the Italian Ministry of University and Research [grant nos RF07.96M2, 020903305]. D. De Zio is a FILAS-Regione Lazio fellow.

Supplementary material available online at
http://jcs.biologists.org/lookup/suppl/doi:10.1242/jcs.086298/-/DC1

References

Besse, B., Cande, C., Spano, J. P., Martin, A., Khayat, D., Le Chevalier, T., Tursz, T., Sabatier, L., Soria, J. C. and Kroemer, G. (2004). Nuclear localization of apoptosis protease activating factor-1 predicts survival after tumor resection in early-stage non-small cell lung cancer. *Clin. Cancer Res.* **10**, 5665-5669.

Catz, S. D. and Johnson, J. L. (2001). Transcriptional regulation of bcl-2 by nuclear factor kappa B and its significance in prostate cancer. *Oncogene* **20**, 7342-7351.

Cecconi, F., Alvarez-Bolado, G., Meyer, B. I., Roth, K. A. and Gruss, P. (1998). Apaf1 (CED-4 homolog) regulates programmed cell death in mammalian development. *Cell* **94**, 727-737.

Cozzolino, M., Ferraro, E., Ferri, A., Rigamonti, D., Quondamatteo, F., Ding, H., Xu, Z. S., Ferrari, F., Angelini, D. F., Rotilio, G. et al. (2004). Apoptosome inactivation rescues proneural and neural cells from neurodegeneration. *Cell Death Differ.* **11**, 1179-1191.

Danial, N. N. and Korsmeyer, S. J. (2004). Cell death: critical control points. *Cell* **116**, 205-219.

Fant, X., Gnadt, N., Haren, L. and Merdes, A. (2009). Stability of the small gamma-tubulin complex requires HCA66, a protein of the centrosome and the nucleolus. *J. Cell Sci.* **122**, 1134-1144.

Ferraro, E., Pulicati, A., Cencioni, M. T., Cozzolino, M., Navoni, F., di Martino, S., Nardacci, R., Carri, M. T. and Cecconi, F. (2008). Apoptosome-deficient cells lose cytochrome c through proteasomal degradation but survive by autophagy-dependent glycolysis. *Mol. Biol. Cell* **19**, 3576-3588.

Frezza, C., Cipolat, S. and Scorrano, L. (2007). Organelle isolation: functional mitochondria from mouse liver, muscle and cultured fibroblasts. *Nat. Protoc.* **2**, 287-295.

Fukasawa, K. (2007). Oncogenes and tumour suppressors take on centrosomes. *Nat. Rev. Cancer* **7**, 911-924.

Gonczy, P. (2004). Centrosomes: hooked on the nucleus. *Curr. Biol.* **14**, R268-R270.

Haren, L., Remy, M. H., Bazin, I., Callebaut, I., Wright, M. and Merdes, A. (2006). NEDD1-dependent recruitment of the gamma-tubulin ring complex to the centrosome is necessary for centriole duplication and spindle assembly. *J. Cell Biol.* **172**, 505-515.

Hausmann, G., O'Reilly, L. A., van Driel, R., Beaumont, J. G., Strasser, A., Adams, J. M. and Huang, D. C. (2000). Pro-apoptotic apoptosis protease-activating factor 1 (Apaf-1) has a cytoplasmic localization distinct from Bcl-2 or Bcl-x(L). *J. Cell Biol.* **149**, 623-634.

Hehnly, H. and Stamnes, M. (2007). Regulating cytoskeleton-based vesicle motility. *FEBS Lett.* **581**, 2112-2118.

Jahani-Asl, A., Germain, M. and Slack, R. S. (2010). Mitochondria: joining forces to thwart cell death. *Biochim Biophys. Acta.* **1802**, 162-166.

Jaspersen, S. L. and Stearns, T. (2008). Exploring the pole: an EMBO conference on centrosomes and spindle pole bodies. *Nat. Cell Biol.* **10**, 1375-1378.

Kodani, A. and Sutterlin, C. (2008). The Golgi protein GM130 regulates centrosome morphology and function. *Mol. Biol. Cell* **19**, 745-753.

Livak, K. J. and Schmittgen, T. D. (2001). Analysis of relative gene expression data using real-time quantitative PCR and the 2(-delta delta C(T)) method. *Methods* **25**, 402-408.

Lotem, J. and Sachs, L. (1995). Regulation of bcl-2, bcl-XL and bax in the control of apoptosis by hematopoietic cytokines and dexamethasone. *Cell Growth Differ.* **6**, 647-653.

Luders, J., Patel, U. K. and Stearns, T. (2006). GCP-WD is a gamma-tubulin targeting factor required for centrosomal and chromatin-mediated microtubule nucleation. *Nat. Cell Biol.* **8**, 137-147.

Malone, C. J., Misner, L., Le Bot, N., Tsai, M. C., Campbell, J. M., Ahringer, J. and White, J. G. (2003). The C. elegans hook protein, ZYG-12, mediates the essential attachment between the centrosome and nucleus. *Cell* **115**, 825-836.

Mazia, D. (1987). The chromosome cycle and the centrosome cycle in the mitotic cycle. *Int. Rev. Cytol.* **100**, 49-92.

Mouhamad, S., Galluzzi, L., Zermati, Y., Castedo, M. and Kroemer, G. (2007). Apaf-1 deficiency causes chromosomal instability. *Cell Cycle* **6**, 3103-3107.

Noritake, J., Watanabe, T., Sato, K., Wang, S. and Kaibuchi, K. (2005). IQGAP1: a key regulator of adhesion and migration. *J. Cell Sci.* **118**, 2085-2092.

Oegema, K., Wiese, C., Martin, O. C., Milligan, R. A., Iwamatsu, A., Mitchison, T. J. and Zheng, Y. (1999). Characterization of two related Drosophila gamma-tubulin complexes that differ in their ability to nucleate microtubules. *J. Cell Biol.* **144**, 721-733.

Padmakumar, V. C., Libotte, T., Lu, W., Zaim, H., Abraham, S., Noegel, A. A., Gotzmann, J., Foisner, R. and Karakesisoglou, I. (2005). The inner nuclear membrane protein Sun1 mediates the anchorage of Nesprin-2 to the nuclear envelope. *J. Cell Sci.* **118**, 3419-3430.

Park, S. H. and Blackstone, C. (2010). Further assembly required: construction and dynamics of the endoplasmic reticulum network. *EMBO Rep.* **11**, 515-521.

Piddubnyak, V., Rigou, P., Michel, L., Rain, J. C., Geneste, O., Wolkenstein, P., Vidaud, D., Hickman, J. A., Mauviel, A. and Poyet, J. L. (2007). Positive regulation of apoptosis by HCA66, a new Apaf-1 interacting protein, and its putative role in the physiopathology of NF1 microdeletion syndrome patients. *Cell Death Differ.* **14**, 1222-1233.

Rai, R., Phadnis, A., Haralkar, S., Badwe, R. A., Dai, H., Li, K. and Lin, S. Y. (2008). Differential regulation of centrosome integrity by DNA damage response proteins. *Cell Cycle* **7**, 2225-2233.

Rieder, C. L., Faruki, S. and Khodjakov, A. (2001). The centrosome in vertebrates: more than a microtubule-organizing center. *Trends Cell Biol.* **11**, 413-419.

Ruiz-Vela, A., Albar, J. P. and Martinez, C. A. (2001). Apaf-1 localization is modulated indirectly by Bcl-2 expression. *FEBS Lett.* **501**, 79-83.

Ruiz-Vela, A., Gonzalez de Buitrago, G. and Martinez, A. C. (2002). Nuclear Apaf-1 and cytochrome *c* redistribution following stress-induced apoptosis. *FEBS Lett.* **517**, 133-138.

Salpingidou, G., Smertenko, A., Hausmanowa-Petrucewicz, I., Hussey, P. J. and Hutchison, C. J. (2007). A novel role for the nuclear membrane protein emerin in association of the centrosome to the outer nuclear membrane. *J. Cell Biol.* **178**, 897-904.

Scorrano, L. (2009). Opening the doors to cytochrome c: changes in mitochondrial shape and apoptosis. *Int. J. Biochem. Cell Biol.* **41**, 1875-1883.

Sevilla, L., Zaldumbide, A., Pognonec, P. and Boulukos, K. E. (2001). Transcriptional regulation of the bcl-x gene encoding the anti-apoptotic Bcl-xL protein by Ets, Rel/NFkappaB, STAT and AP1 transcription factor families. *Histol. Histopathol.* **16**, 595-601.

Sun, Y., Orrenius, S., Pervaiz, S. and Fadeel, B. (2005). Plasma membrane sequestration of apoptotic protease-activating factor-1 in human B-lymphoma cells: a novel mechanism of chemoresistance. *Blood* **105**, 4070-4077.

Thyberg, J. and Moskalewski, S. (1999). Role of microtubules in the organization of the Golgi complex. *Exp. Cell Res.* **246**, 263-279.

Varadi, A., Johnson-Cadwell, L. I., Cirulli, V., Yoon, Y., Allan, V. J. and Rutter, G. A. (2004). Cytoplasmic dynein regulates the subcellular distribution of mitochondria by controlling the recruitment of the fission factor dynamin-related protein-1. *J. Cell Sci.* **117**, 4389-4400.

Wang, X. (2001). The expanding role of mitochondria in apoptosis. *Genes Dev.* **15**, 2922-2933.

Watanabe, T., Noritake, J. and Kaibuchi, K. (2005). Regulation of microtubules in cell migration. *Trends Cell Biol.* **15**, 76-83.

Zermati, Y., Mouhamad, S., Stergiou, L., Besse, B., Galluzzi, L., Boehrer, S., Pauleau, A. L., Rosselli, F., D'Amelio, M., Amendola, R. et al. (2007). Nonapoptotic role for Apaf-1 in the DNA damage checkpoint. *Mol. Cell* **28**, 624-637.

Zou, H., Henzel, W. J., Liu, X., Lutschg, A. and Wang, X. (1997). Apaf-1, a human protein homologous to C. elegans CED-4, participates in cytochrome c-dependent activation of caspase-3. *Cell* **90**, 405-413.

Journal of Cell Science